Macromolecules
ARTICLE

Macromolecules **2010**, *43*, 3027–3035 **3027**
DOI: 10.1021/ma9027239

Coil-Collapse and Coil-Aggregation due to the Interaction of Cu^{2+} and Ca^{2+} Ions with Anionic Polyacylate Chains in Dilute Solution

S. Lages, R. Michels, and K. Huber*

Department Chemie, Universität Paderborn, Fakultät für Naturwissenschaften, Warburger Strasse 100, D-33098 Paderborn, Germany

Received December 11, 2009; Revised Manuscript Received February 15, 2010

ABSTRACT: A detailed light scattering investigation is presented on dilute solutions of long chain sodium polyacrylate in the presence of Cu^{2+} ions under conditions which are close to the precipitation threshold of the respective Cu^{2+}−PA chains. The results are compared with literature data (*Eur. Phys. J E* **2001**, *5*, 117−126) from the corresponding system in the presence of Ca^{2+} ions. In all cases the solvent is a 0.1 M NaCl solution in water. The PA coils shrink considerably with increasing Cu^{2+} concentration as the conditions approach the precipitation threshold. Yet, the extent of shrinking can not be driven as far as for the respective Ca^{2+}−PA system, where fully collapsed sphere-like polymers had been observed at the threshold. Analysis of the aggregation process with time-resolved static light scattering reveals loose coil-like aggregate structures for Cu^{2+}−PA aggregates and compact sphere-like aggregates for Ca^{2+}−PA in accordance with the limiting shape of the respective shrunken single chains. The onset of Ca^{2+} or Cu^{2+} induced aggregation of PA chains at the precipitation threshold borders an intramolecular coil shrinking process. The transition of shrinking into aggregation occurs more readily with Cu^{2+}−PA as it does with Ca^{2+}−PA.

Introduction

Interactions of polyelectrolyte chains with simple salts like NaCl in aqueous solution are dominated by electrostatic forces. These interactions cause counterion condensation and with it a screening of the electrostatic repulsions among the charges of the highly charged polyelectrolyte chains. As a consequence, coil dimensions shrink and eventually pass the state of unperturbed dimensions as the salt concentration is increased.[1−3] At very high salt concentration, the coils may precipitate denoted as salting out.

Unlike to these predominantly electrostatic interactions observed with simple salts, bivalent alkaline earth cations or transition metal cations exhibit specific interactions with various polyelectrolytes. A large extent of work has been published on the interactions of alkaline earth cations with anionic polycarboxylate chains. Addition of the respective alkaline earth salts to dilute solutions of sodium polyacrylate (NaPA) coils causes a coil shrinking, which reaches a compact sphere-like shape if a critical salt concentration is achieved.[4−8] Further addition of alkaline earth cations causes a macroscopic precipitation of the polyacrylate. Most strikingly, this critical alkaline earth cation concentration increases stoichiometrically with the content of polyanions in solution, leading to a linear phase boundary.[4,9−12] Addition of a simple salt like NaCl causes a partial ion exchange at the COO^- residues of the polymer backbone and thus leads to a chain re-expansion and to an expansion of the stability regime of the complexes of polyacrylate chains with the respective alkaline earth cations.[6,9]

Compared to the detailed picture established for the morphological changes of polycarboxylate chains interacting with alkaline earth cations, the impact of transition metal cations on the shape of these chains is less well understood. An investigation of NaPA with Ag^+ ions in aqueous solution at a salt level of 0.01 M $NaNO_3$ revealed already a shrinking of the PA coils by a factor of $^1/_2$ if a few percent of the COO^- groups were decorated by Ag^+ cations, indicating an impact of these monovalent transition metal cations which is much stronger than the one exerted by alkaline earth cations.[13] However, further shrinking was prevented by the onset of a competing aggregation of interacting coils. Above all, investigation of morphological changes of coil conformation was distorted by the formation of silver nanoparticles induced by exposure to light.

The first paper known to address interactions of polycarboxylates with Cu^{2+} ions was published in 1954 by Flory and Osterheld.[14] The authors could clearly show that Cu^{2+} ions are more effective than Na^+ or even Ca^{2+} ions in suppressing the typical viscosity increase of anionic NaPA in dilute solution. A few decades later, interest in morphological transformations of polycarboxylates induced by Cu^{2+} ions revived. Heitz and Francois revealed a considerable shrinking of nondissociated polymethacrylic acid upon addition Cu^{2+} ions.[15] Although, the polymethacrylic acid coils expanded due to neutralization, the dimensions kept always much lower if Cu^{2+} ions were present in solution. Supplementary small-angle X-ray scattering revealed a maximum in the Kratky plot if copper ions were present in solution, indicating a considerable degree of coil compaction. In a highly systematic investigation, Rühe et al.[16] induced a shrinking of NaPA brushes through exposure to solutions of various cations and postulated three modes of interaction for the NaPA brush with the metal cations, (i) electrostatic screening by inert salts; (ii) specific interactions with dehydration and (iii) specific interactions with bridging. In this scheme, Cu^{2+} ions follow the third mode of interaction, leading to a shrinking of the brush at much lower Cu^{2+} concentrations than revealed with alkaline earth cations, yet at a slightly lower extent of shrinkage than observed with alkaline earth cations. The strong propensity of compaction induced by copper ions was interpreted by the formation of bridging binucleate Cu^{2+}−Cu^{2+} complexes[15,16] as one of two types of binding between the COO^- ligands of polycarboxylates and Cu^{2+} ions meanwhile established. The two types of binding are mononuclear bidentate complexes and binuclear complexes, which bridge remote chain segments via four COO^-

*Corresponding author.

Published on Web 03/01/2010

residues binding to a pair of Cu^{2+} ions.[17−19] In the latter case, the COO^- ligands interconnect two Cu^{2+} ions whereby the two oxygen atoms bind to different copper ions, respectively. Bokias et al.[20] investigated the variation of the fraction of bound Cu^{2+} and its distribution among the two types of complexes at a variable ratio $[Cu^{2+}]/[COO^-]$ and at fixed degrees of dissociation of the poly(acrylic acid)respectively.

Shrinking experiments on dilute polycarboxylate coils similar to those with Ag^+ and alkaline earth cations[6−8,13] were also performed with Cu^{2+} ions interacting with anionic polymethacyrlate (NaPMA) chains in 0.1 M NaCl.[21] The experiments were more successful than those with Ag^+ because no reduction of copper ions interfered with their interaction to PMA. Compared to the impact of alkaline earth cations, the observed interaction of Cu^{2+} ions was strong enough to suppress ion exchange effects, even at an inert salt level of 0.1 M NaCl. As shown by light scattering, the extent of shrinking was largest close to the precipitation threshold of the respective Cu^{2+}−PMA. The shrinking trends depended only on the ratio of Cu^{2+} to COO^-, suggesting a stoichiometry of 1:2 for the complex,[21] which was confirmed later by Bokias et al.[20] Another important result was that the values of the structure-sensitive ratio ρ of the radius of gyration R_g over the hydrodynamically effective radius R_h scattered around $1.5 < \rho < 2.0$, independent of the degree of coil shrinking. Such high and constant values are typical for extended coils with a polydisperse mass distribution. This constancy can be interpreted by two alternative modes of shrinking: (i) a self-similar process or alternatively (ii) a cascade of intermediates with shrunken pearl-like subsegments along the remaining contour. However, this preliminary investigation on NaPMA does not allow a quantitative comparison with our detailed knowledge, established for the shrinking of NaPA chains induced by alkaline earth cations. As an additional advantage compared to NaPMA, unperturbed dimensions are available for aqueous NaPA, helping to better quantify the extent of shrinking relative to the unperturbed dimensions of the respective chains.

The present piece of work resumes our preliminary results on Cu^{2+}−PMA by systematically investigating the shrinking of long chain NaPA coils induced by the addition of Cu^{2+} ions. The molar mass of NaPA was 2800 kDa. Combined static and dynamic light scattering are applied as analytical methods, which will not only quantify the size of the shrinking coils but will also give indications for their shape as it makes accessible a comparison of the radius of gyration with the corresponding hydrodynamic radius. The shrinking is induced with the same technique successfully applied for our detailed analysis of the interactions between NaPA chains and alkaline earth cations,[6,8] i.e. the phase boundary where the corresponding Cu^{2+}−PA precipitates is approached by increasing the ratio of $[Cu^{2+}]/[COO^-]$. The medium is an aqueous solution with 0.1 M NaCl. The added NaCl screens interparticle interactions and enables interpretation of scattering data in terms of single chain behavior. The results will supplement our knowledge on NaPA coil shrinking and enable a direct comparison of the impact of alkaline earth cations with the impact of Cu^{2+} ions. Beyond this, the present work investigates for the first time the onset of aggregation of M^{2+}−PA coils, once the phase boundary is crossed. The latter investigation will be performed by time-resolved static light scattering (TR-SLS) experiments and is expected to offer insight into the mechanism of the aggregation of shrunken M^{2+}−PA coils with M^{2+} corresponding to Cu^{2+} or Ca^{2+} and to relate this insight with the observed mode of chain shrinking induced by the respective cation.

Experimental Section and Data Evaluation

Materials. NaCl, $CuCl_2 \cdot 2H_2O$, and solid NaOH of analytical grade were purchased from Fluka (Buchs, Switzerland). Aqueous solutions thereof were prepared with bidistilled water with a conductivity < 0.1 μS. The sodium polyacrylate P1300 was purchased from Polysciences (Eppelheim, Germany). All solutions were purified from dust prior to scattering experiments by filtration with syringe filters from Millipore (Eschborn, Germany) using 0.22 μm CA filters for the solvents and 0.45 μm PVDF filters for the NaPA solutions. Cylindrical scattering cells from Hellma (Müllheim, Germany) with an outer diameter of 20 mm or 25 mm were used for the combined dynamic and static light scattering experiments (DLS and SLS) and for the time-resolved static light scattering experiments (TR-SLS), respectively.

Combined DLS and SLS Experiments. Combined LS experiments were performed using a model 5000E compact goniometer system from ALV-Laser Vertriebsgesellschaft (Langen, Germany), equipped with a Nd:YAG laser with 200 mW operating at a wavelength of 532 nm. A C25 Haake bath was used to set the temperature to 25 °C with a precision of 0.01 °C. The scattering intensities were recorded in an angular regime of $30° \leq \theta \leq 150°$.

The NaPA standard P1300 was characterized in an aqueous solution of 0.1 M (0.1 mol/L) NaCl at a pH of 9 by combined static and dynamic light scattering at 25 °C. Four concentrations have been analyzed in a regime of $0.179 \times 10^{-4}\ nm^{-2} < q^2 < 1.878 \times 10^{-4}\ nm^{-2}$ according to a procedure already used by Schweins et al.[3] The procedure yielded a mass averaged molar mass $M_w = 2800$ kDa, a radius of gyration $R_g = 184$ nm and a hydrodynamically effective radius $R_h = 128$ nm established from the z-averaged diffusion coefficient. The diffusion coefficient was evaluated by Koppel's cumulant method[22] which gave in addition a relative dispersion of the diffusion coefficient of $\mu_2/\Gamma^2 = 1.25$ about its z-average. The latter value was established as an extrapolation to $c = 0$. The refractive index n, the viscosity η and the refractive index increment $(\partial n/\partial c)_\mu$ necessary for the data evaluation of NaPA in 0.1 M NaCl solution are[3] $n = 1.336$, $\eta = 0.8979$ mPa·s and $(\partial n/\partial c)_\mu = 0.167$ mL/g. The index μ at $(\partial n/\partial c)_\mu$ indicates that the dn/dc of NaPA was determined at the constant chemical potential corresponding to a 0.1 M NaCl solution.[3]

A stock solution of the NaPA standard P1300 in 100 mmol/L (0.1M) aqueous NaCl as solvent was prepared and gently mixed at room temperature for 3 days. The pH of the aqueous NaCl solution was set to 9 using 100 mM aqueos NaOH prior to dissolving the NaPA. A second salt solution with a total cation molarity $[C] = [Na^+] + 2 \cdot [Cu^{2+}] = 100$ mM of cationic charges was prepared in bidistilled water. Because of the formation and precipitation of colloidal $Cu(OH)_2$ the pH of this solution was not manipulated. By adding the appropriate amounts of the NaPA stock solution and the Cu^{2+} containing salt solution in graduated flasks, five series with NaPA concentrations of 0.11, 0.22, 0.27, 0.32, and 0.39 mM expressed as monomer concentrations [PA], were prepared. In each of this series with constant NaPA concentration, the Cu^{2+} concentration was set to 0.01, 0.02, 0.03, 0.04, 0.05, and 0.06 mM giving a total amount of 30 samples with pH values between $7.0 \leq pH \leq 7.3$. The solutions were gently mixed at room temperature for 12 h.

The scattering experiments on M^{2+} induced coil shrinking were carried out at 25 °C. Extrapolation to zero concentration was not possible because the coil-size effects under consideration depend on the PA concentration as its variation modifies the ratio $[Cu^{2+}]/[PA]$. The angular dependent SLS experiments were evaluated according to Zimm's approximation[23] in a regime of $0.661 \times 10^{-4}\ nm^{-2} < q^2 < 4.93 \times 10^{-4}\ nm^{-2}$ by extrapolating to zero scattering angle, resulting in an apparent weight-averaged molar mass M_w and an apparent radius of gyration R_g:

$$\frac{Kc}{\Delta R_\theta} \cong \frac{1}{M_w} + \frac{R_g^2 q^2}{3M_w} \quad (1)$$

In eq 1, K is the contrast factor, c the polymer concentration in g/L, ΔR_θ the excess scattering intensity of the polymeric

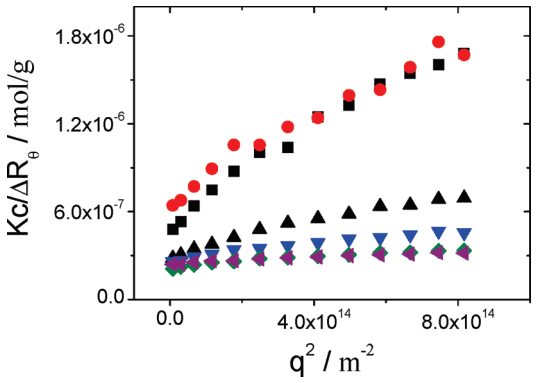

Figure 1. SLS data at a NaPA concentration of 0.11 mM. The copper concentrations are 0.01 (black box), 0.02 (red circle), 0.03 (black triangle, pointing up), 0.04 (blue triangle, pointing down), 0.05 (green tilted square), and 0.06 mM (purple triangle, pointing left).

solute and q the scattering vector magnitude.

$$K = \frac{4\pi^2}{\lambda_0^4 N_A}\left(n\left(\frac{\partial n}{\partial c}\right)_\mu\right)^2 \quad (2)$$

In eq 2, $\lambda_0 = 532$ nm is the vacuum wavelength of the laser, N_A is Avogadro's number, $n = 1.336$ is the refractive index of the solvent and $(\partial n/\partial c)_\mu = 0.167$ mL/g is the refractive index increment of NaPA in aqueous NaCl with the chemical potential of 0.1 mM NaCl in this case. With θ being the scattering angle, the scattering vector q is defined as:

$$q = \frac{4\pi n}{\lambda_0}\sin\frac{\theta}{2} \quad (3)$$

By extrapolating to zero scattering angle, the DLS experiments were evaluated according to

$$D \cong D_z(1 + CR_g^2 q^2) \quad (4)$$

D in eq 4, like $Kc/\Delta R_\theta$ in eq1 could not be extrapolated to c equal zero and is thus an apparent diffusion coefficient. It was evaluated using the cumulant method[22] including linear and quadratic powers of the correlation time t. According to the Stokes−Einstein relation, D can be transformed into a hydrodynamically effective radius R_h:

$$R_h = \frac{k_B T}{6\pi \cdot \eta \cdot D} \quad (5)$$

In eq 5 k_B is Boltzmann's constant, T is the absolute temperature and $\eta = 0.860$ mPa·s is the viscosity of the solvent.

Although, R_g and R_h are apparent values, the deviation from the true size values is considered to be negligibly small and even disappears at the collapse point because the decoration of the coils with M^{2+} screens interparticular interactions.

Impairment of the analysis of single particle shrinking pattern by a premature onset of aggregation could be excluded as only those samples have been used in which apparent molar mass values did not significantly deviate from the apparent value measured far off the phase boundary. If aggregate formation would have occurred to a significant extent two possible mass deviations have to be considered. A significant increase in mass is observed if the aggregates would have been formed after filtration or if the aggregates would have passed the filters. A significant decrease in mass values is recorded if the aggregates would have been removed by filtration. None of these effects have been observed with the samples discussed in Figures 2−4.

Construction of the Phase Boundary. The phase boundary of Cu^{2+}−NaPA in 0.1 M NaCl was constructed in analogy to a

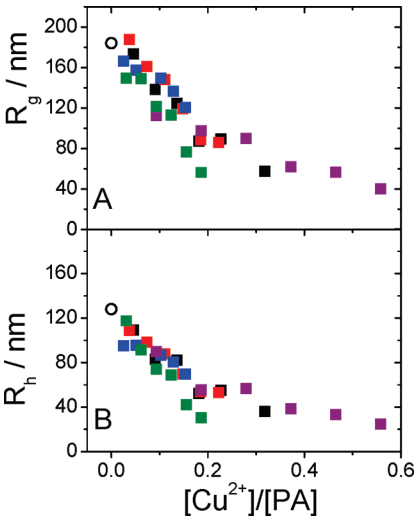

Figure 2. R_g values (A) and R_h values (B) plotted versus the ratio $[Cu^{2+}]/[PA]$ of the molar ion concentration $[Cu^{2+}]$ to the monomeric molar monomer concentration [PA] of NaPA. The symbols denote copper concentration series at NaPA concentrations of 0.11 (purple box), 0.22 (black box), 0.27 (red box), 0.32 (green box), and 0.39 mM (blue box). The copper concentrations in each series are 0.01, 0.02, 0.03, 0.04, 0.05, and 0.06 mM. The open circle indicates the reference state of the NaPA coils in copper free solution.

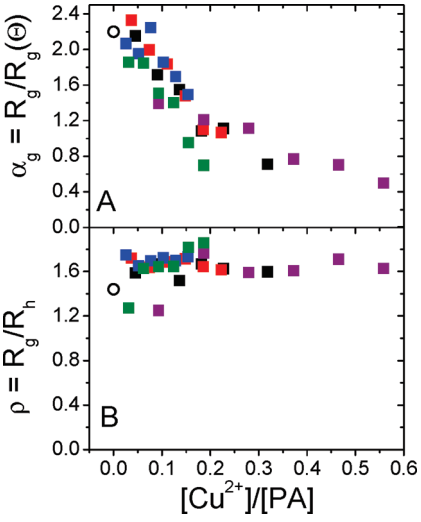

Figure 3. Extent of coil shrinking α_g (A) and structure-sensitive parameter ρ (B) plotted versus the ratio of the molar Cu^{2+} ion concentration $[Cu^{2+}]$ to the monomeric molar NaPA concentration [PA], $[Cu^{2+}]/[PA]$. The symbols denote copper concentration series at NaPA concentrations of 0.11 mM (purple box), 0.22 mM (black box), 0.27 mM (red box), 0.32 mM (green box) and 0.39 mM (blue box). The copper concentrations in each series are 0.01, 0.02, 0.03, 0.04, 0.05, and 0.06 mM. The open circle indicates the reference state of the NaPA coils in copper free solution.

procedure originally introduced[4] for the system Ca^{2+}−PA. Construction is based on the assumption that the state of the collapsed NaPA coil approaches a compact sphere at the phase boundary. The radius R of this sphere was estimated to $R_o = 16.2$ nm using the appropriate degree of polymerization $DP = M_w/M_0 = 2.8 \times 10^6/94 = 29800$ and a volume of monomeric unit of 0.6 nm^3. Plotting the logarithm of the hydrodynamically effective radius R_h against the Cu^{2+} concentration within each series of constant NaPA concentration reveals a linear correlation. Extrapolation to $\log(R_0/\text{nm}) = \log(16.2) = 1.21$ (inlet of Figure 5) yields the critical Cu^{2+} concentration for the respective series.

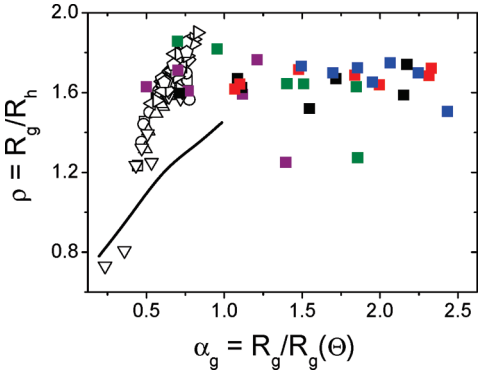

Figure 4. Structure-sensitive parameter ρ plotted versus the extent of coil shrinking α_g. The symbols denote copper concentration series at NaPA concentrations of 0.11 (purple box), 0.22 (black box), 0.27 (red box), 0.32 (green box), and 0.39 mM (blue box). The copper concentrations in each series are 0.01, 0.02, 0.03, 0.04, 0.05, and 0.06 mM. Open symbols show the shrinking behavior of NaPA in 0.1 M NaCl in the presence of Ca^{2+} ions.[6] The black line shows the shrinking behavior of poly(*N*-isopropylacrylamid) (PNIPAM) in aqueous solution.[30] PNIPAM is a good comparison, because it is a neutral derivate of NaPA.

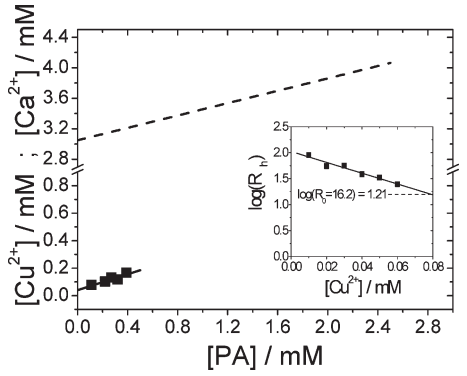

Figure 5. Phase boundary of NaPA in the presence of Ca^{2+} ions (--) and in the presence of Cu^{2+} ions (■). The straight line (—) is a linear fit to the data (■). The inlet illustrates the evaluation of the critical Cu^{2+} concentration at [PA] = 0.11 mM as the intersection of a linear fit to a plot of log(R_h) vs [Cu^{2+}] to $R_h = R_0 = 16.2$ nm.

TR-SLS Experiments. The scattering curves are recorded with a home-build goniometer system[24] equipped with a He−Ne laser operating at 632 nm and a power of 30 mW. The instrument allows the simultaneous detection of static light scattering curves at 2 × 19 fixed angles arranged in pairs on both sides of the beam symmetrically in an angular regime of 25.84° ≤ Θ ≤ 143.13°. A C25 Haake bath was used to set the temperature to 25 °C. Each scattering curve was based on 4000 measurements each requiring a recording time of 0.002 s. Taking into account the time required to process the raw data, the smallest possible time increment for the recording of one scattering curve with this setup is $\Delta t \approx 30$ s. An occasionally appearing signal overflow at a certain angle led to an elimination of the respective angular signal.[26] The same refractive index and refractive index increment have been used at 532 nm and at 632 nm. This can be justified because the refractive index increments at 532 nm and at 632 nm only differ by about 0.1%.[3]

The aggregation experiment with Cu^{2+} was performed twice and denoted as Cu01 and Cu02. 5.0 mL of a solution of NaPA in 100 mM aqueous NaCl with a NaPA concentration of 0.217 mM were filtered into a Hellma scattering cell. The TR-SLS experiment respectively indicated by the suffix "-a" in the sample name in Table 1 was performed after the first addition of 50 μL of a solution which is 5.05 mM with Cu^{2+} ions and 89.9 mM with Na^+ ions. The sample volume in the scattering cell was now 5.05 mL and the NaPA and the Cu^{2+} concentration were 0.215 and 0.05 mM, respectively. The phase boundary was crossed by further stepwise addition of the Cu^{2+} solution. In each step, 50 μL of a dust free solution containing 5.05 mM Cu^{2+} ions and 89.9 mM Na^+ ions were added to the scattering cuvette by using an Eppendorf pipet. Within 30 s, the cuvette was placed into the goniometer and the measurement was started, respectively. The scattering curves were recorded with $\Delta t = 40$ s between two successive curves. The NaPA concentration in the scattering cell decreased only slightly by this procedure and amounted to 0.211 mM after the final step while the Cu^{2+} concentration reached a value of 0.147 mM in the experimental series Cu01. In the case of experimental series Cu02, the aggregation process did not set in at this concentrations and an additional portion of 50 μL of the Cu^{2+} solution became necessary to start the aggregation process. In this case the final NaPA and Cu^{2+} concentrations in the scattering cell were 0.209 and 0.194 mM, respectively. Because of the increasing scattering signal accompanied by a strong signal overflow, the measurement of the aggregation step was stopped after 20 min.

Table 1. Overview on the Aggregation Experiments of M^{2+}−PA in 0.1 M NaCl

experiment	[NaPA]/mM	[M^{2+}]/mM	R_g/nm	R_h/nm	$\rho = R_g/R_h$
Cu01-a	0.215	0.050	82.3[a] 90.9[b]	50.9[b]	1.79[b]
Cu01-b	0.213	0.099	110.2[a] 115.0[b]	75.1[b]	1.53[b]
Cu01-c	0.211	0.147	109.3[c]		
Cu02-a	0.211	0.147	62.3[a]		
Cu02-b	0.209	0.194	76.5[c]		
Ca01-a	1.032	3.271	70.6[a] 72.4[b]	37.3[b]	1.94[b]
Ca01-b	1.021	3.704	67.1[c]		
Ca02-a	0.960	3.899	70.6[a]		
Ca02-b	0.957	4.029	66.8[c]		
Ca03-a	0.183	3.963	183.0[a]		
Ca03-b	0.188	4.602	61.0[c]		
Ca04-a	0.957	4.029	114.0[a]		
Ca04-b	0.953	4.158	65.9[c] 136.6[d]	176.8[d]	0.773[d]

[a] Results from TR-SLS experiments. [b] Results from combined DLS and SLS experiments. [c] First R_g value measured via TR-SLS at the beginning of the aggregation process. [d] Results from combined DLS and SLS experiments during the aggregation process.

The aggregation experiments with calcium ions were performed in a similar way. In the case of experimental series Ca01, 5.0 mL of NaPA in 100 mM aqueous NaCl with a NaPA concentration of 1.087 mM were filtrated into the scattering cell. A dust free solution, containing 50 mM $CaCl_2$ was added with an Eppendorf pipet in steps of 50 μL. The experimental series Ca02 and Ca04 started with a slightly lower NaPA concentration of 1.024 mM. In both series, a dust free solution containing 40 mM $CaCl_2$ and 20 mM NaCl was added to the respective scattering cell in increments of 100 μL first and later 20 μL with an Eppendorf pipet. In the case of the experimental series Ca03, the concentration of the Ca^{2+} free NaPA solution was 0.213 mM, which is close to the concentrations of the series with Cu^{2+}. A dust free solution containing 40 mM $CaCl_2$ and 20 mM NaCl was added in steps of 100 and 50 μL. In the experimental series Ca03 the aggregation process set in at [PA] = 0.188 mM and [Ca^{2+}] = 4.602 mM. The values $n = 1.336$ and $(\partial n/\partial c)_\mu = 0.167$ mL/g were applied respectively as refractive index of the solvent and as the refractive index increment of NaPA at a chemical potential corresponding to 0.1 M NaCl.

Evaluation of the TR-SLS data for the aggregation experiments induced by Cu^{2+} cations was performed with an analysis according to eq1 in a regime of $0.7 \times 10^{-4}\text{nm}^{-2} < q^2 < 2.82 \times 10^{-4}\text{nm}^{-2}$. All scattering curves recorded for these aggregation processes turned out to follow straight lines in the respective *q*-regime. This holds for polydisperse coil-like structures and certain branched structures as is demonstrated in the Supporting Information. A quadratic fit which includes an additional q^4 term in eq1 gives only slightly larger R_g and M_w values than the

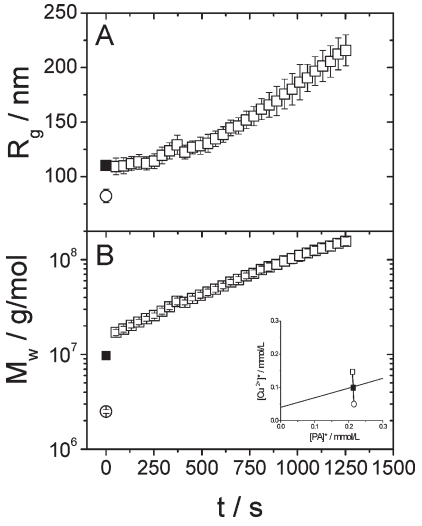

Figure 6. R_g (A) and M_w (B) for samples Cu01-a (○), Cu01-b (■), and Cu01-c (□). The inlet shows the respective trajectory in the phase diagram. Further details of the sample characteristics are given in Table 1.

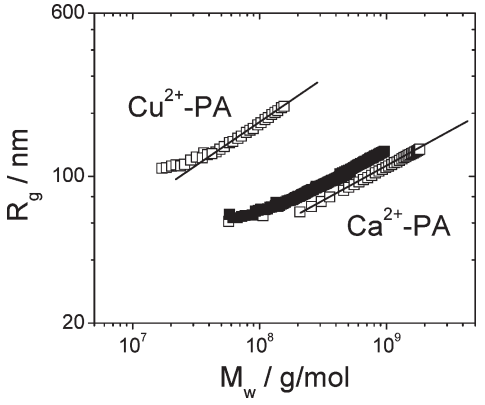

Figure 7. Plot of the radius of gyration against weight-averaged molar mass for the experiments Cu01-c (□), Ca03-b (□), and Ca04-b (■). The solid line to Cu01-c corresponds to an exponent of 0.40 extracted above $M_{w,app} = 4.2 \times 10^7$ g/mol ($t > 530$ in Figure 6) and the solid line to Ca03-b has a slope of 0.32 if established above $M_{w,app} = 2.0 \times 10^8$ g/mol.

corresponding linear fit does without having any effect on the mass versus size correlations. The TR-SLS data for the aggregation experiments with Ca^{2+} cations turned out to be most suitably analyzed according to Guinier's approximation[25] in a regime of 0.352×10^{-4} nm$^{-2} < q^2 < 3.17 \times 10^{-4}$ nm^{-2}

$$\ln\left(\frac{Kc}{\Delta R_\theta}\right) \cong \ln\left(\frac{1}{M_w P(q)}\right) = \ln\left(\frac{1}{M_w}\right) + \frac{R_g^2 q^2}{3} \qquad (6)$$

with $P(q) \approx \exp\{-(1/3)R_g^2 q^2\}$. As is shown in the Supporting Information, the fit in the respective q-regime gives accurate results for polydisperse spheres. The resulting formfactors represented in Figures 8 and 10 follow characteristic master curves respectively and serve as an additional confirmation of the applied procedures to fit the data.

Results and Discussion

The Coil Collapse. In five series of experiments NaPA chains in dilute solution were shrunken by an increasing content of Cu^{2+} ions. In each series the Cu^{2+} concentration was increased at constant concentrations of NaPA respectively. All series covered a regime of NaPA concentration of

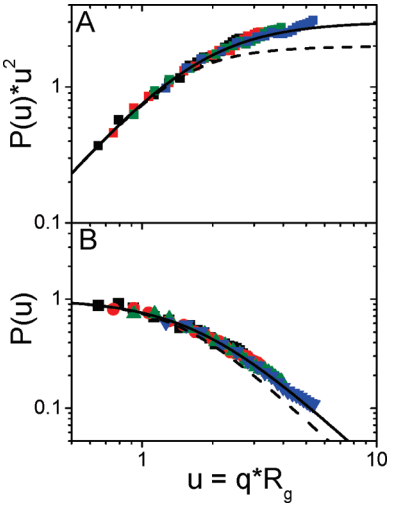

Figure 8. Normailzed Kratky plot (A) and form factor (B) of the scattering data of Cu^{2+}−PA intermediates within series Cu01-c at 50 (black box), 450 (red box), 770 (green box), and 1200 s (blue box). NaPA and Cu^{2+} concentrations are 0.211 and 0.147 mM, respectively. The black line corresponds to the form factor of a Gaussian coil with a polydispersity index PDI = 2.[23,31,32] The dashed curve indicates the respective model curve for monodisperse coils.[31]

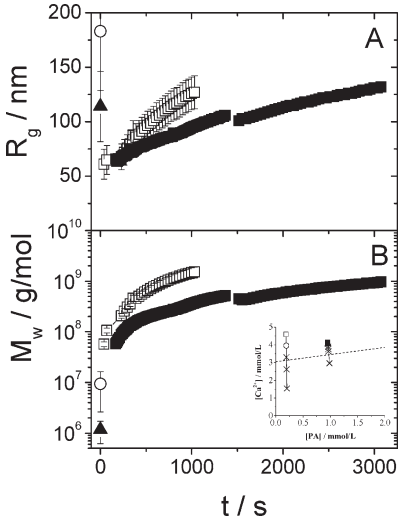

Figure 9. R_g (A) and M_w (B) of the experiments Ca03-a (○), Ca03-b (□), Ca04-a (▲), and Ca04-b (■). The inlet shows the respective trajectory in the phase diagram. Further details of the sample characteristics are given in Table 1.

0.11 mM ≤ [PA] ≤ 0.39 mM as the monomer concentration, corresponding to a concentration of 0.0092 g/L < c < 0.0327 g/L. Figure 1 shows the SLS data of one selected example at [PA] = 0.11 mM as $Kc/\Delta R_\Theta$ versus q^2. The slope of the scattering curves in Figure 1 decreases with increasing copper concentration. Figure 2 summarizes the evolution of the apparent radius of gyration and the apparent hydrodynamically effective radius as a function of the concentration ratio of copper ions per monomeric units expressed as [Cu^{2+}]/[PA]. The apparent size of the anionic PA coils shrinks drastically as the copper concentration increases. Data recorded above [Cu^{2+}]/[PA] = 0.2 seem to indicate a shrinking trend which is considerably weaker than below 0.2. For both radii, the respective variations overlay, suggesting that the ratio of the two ion concentrations is the crucial variable and that the trends point to a single limiting value of [Cu^{2+}]/[PA] at which the system crosses the phase boundary

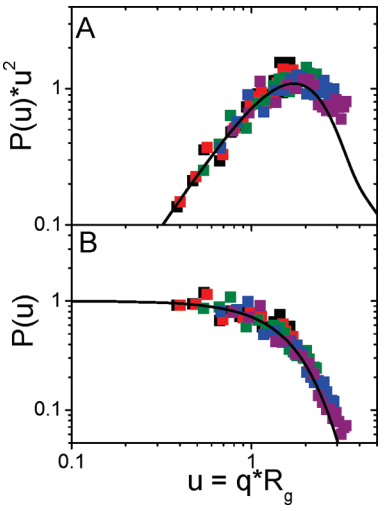

Figure 10. Kratky plot (A) and form factor (B) of the scattering data from Ca^{2+}−PA intermediates of the experimental series Ca03-b at 71 (black box), 230 (red box), 454 (green box), 774 (blue box), and 1190 s (■). The solid black line corresponds to a polydisperse sphere[23,33] with a PDI = 2.

and precipitates. This can be interpreted by a characteristic stoichiometry of COO^- residues per Cu^{2+} ion in the precipitate.

Two parameters can be used to analyze the extent of shrinking and the accompanying morphological changes in the collapsing coils. The first parameter relates the size of the shrinking coil R_g to the radius of gyration of its unperturbed dimensions $R_g(\Theta)$.

$$\alpha_g = R_g/R_g(\Theta) \tag{7}$$

For the present NaPA sample, $R_g(\Theta)$ in eq7 can be estimated according to eq 13b of ref 3, which correlates the radius of gyration to the molar mass of NaPA in an aqueous solution at an inert salt content of [NaCl] = 1.5 M. In the presence of 1.5 M NaCl, NaPA chains adopt their unperturbed dimensions.[1,3] The second parameter compares the ratio of the radius of gyration R_g to the hydrodynamically effective radius R_h of a sample according to

$$\rho = R_g/R_h \tag{8}$$

The ρ-ratio is structure-sensitive.[27] For linear, flexible polymer coils theory predicts a value of $\rho = 1.504$, which increases to 1.86 under good solvent conditions. Polydispersity also increases ρ. The theoretical value at Θ-condition becomes 1.73 if the weight-averaged molecular weight M_w is twice as large as the number-averaged molecular weight M_n. Experimental values for monodisperse linear polymer samples under Θ-conditions are about 15% lower than theoretically predicted.[28] For NaPA in 1.5 M NaCl a value of $\rho = 1.53$ could be established.[3] Homogeneous spheres with a monodisperse size have a value of $\rho = 0.78$, which is significantly smaller than the value for linear chains. The impact of polydispersity in the case of spheres is expected to be much smaller than for linear chains[8] and still negligible at $M_w/M_n = 2$. Thus, discrimination between coils and spheres by means of ρ is possible.

The data shown in Figure 2, enable direct calculation of α_g and ρ with eq7 and 8. Results are presented in Figure 3. All five series of experiments led to a unique decrease of the expansion factor α_g, which approaches 1 at a ratio $[Cu^{2+}]/[PA] = 0.25$. At this value, the coil reaches its unperturbed dimensions and further shrinking occurs more gradually. The strongest degree of shrinking appears at $\alpha_g = 0.5$. It belongs to the series with the lowest polymer concentration. As has already been mentioned, the fact that the shrinking trends from all concentration series overlay, indicates that a critical stoichiometric ratio exists where coil shrinking borders precipitation. If this critical ratio corresponds to the point where the shrinking trend changes its slope, it indicates 4 COO^- residues per bound Cu^{2+} ion and if this critical ratio is close to the largest shrinking extent observed, it indicates only 2 COO^- residues per bound Cu^{2+} ions. As soon as this phase boundary is crossed, aggregation inevitably starts to compete with the intramolecular chain shrinking. Yet, the propensity to aggregate gets weaker, as the NaPA concentration decreases. It has to be emphasized at this point that the extent of shrinking achieved with Ca^{2+} ions under the same conditions[6] exceeded the strongest degree of shrinking observed for Cu^{2+} in the present work.

The corresponding ρ values observed with Cu^{2+} ions scatter around a value close to 1.6 for all five series of experiments. The average value of $\rho = 1.6$ is only slightly larger than the value determined for NaPA under Θ-conditions but lower than the value of $\rho = 1.84$ established in 0.1 M NaCl which corresponds to good solvent conditions.[3] The fact that the ρ values stay close to the value of unperturbed NaPA coils may be interpreted by several alternative shrinking mechanisms for the Cu^{2+}−PA: (i) The shrinking intermediates adopt self-similar shapes resembling closely the shape of an unperturbed coil; (ii) the shrinking process generates a cascade of intermediates with two opposing effects on the ρ-ratio, i.e., an increasing compaction, which decreases ρ and an increasingly anisotropic shape, which increases ρ. The most prominent model, currently discussed for elongated shapes of collapsing polyelectrolyte chains is the necklace-like chain model, with compact pearls interconnected by stretched chain-like strings.[29] Although this model is highly anisotropic as the interconnecting strings form a straight line, it points to still another alternative (iii) where the shrinking also generates locally condensed nodules but now the connecting strings keep their freely jointed chain arrangement albeit with a shorter contour than in the absence of any collapsed domains.

This apparent constancy of the ρ value for the Cu^{2+} induced shrinking compares with a gradual but significant decrease observed for the collapsing Ca−PA chains. Unfortunately, the α_g-regime, covered by data from both cations is only a narrow range in between $0.5 < \alpha_g < 0.8$.[6] For a direct comparison, the present data are replotted as a function of α_g and combined with the respective data from ref 6 measured at [NaCl] = 0.1 M in Figure 4. The data for the Ca^{2+}-induced shrinking even indicated a collapse to spherical particles not observed in the case of the Cu^{2+} induced shrinking. Yet, the major difference between the two cations is that we could reach much lower shrinking ratios with Ca^{2+} ions ($\alpha_g \sim 0.25$) than with Cu^{2+} ions ($\alpha_g \sim 0.5$). In the α_g regime covered by data from both cations in Figure 4, no discrimination between the two trends is possible. As each of the experimental series ended once aggregation and/or precipitation occurred for the first time, aggregation of Cu^{2+}−PA interferes with shrinking already at lower degrees of shrinking than aggregation of Ca^{2+}−PA does.

The experiments enabled us in addition to establish the phase boundary as the threshold between the clear solution state and the state where aggregation and/or precipitation starts. The resulting phase boundary is shown in Figure 5 together with the respective phase boundary of the Ca^{2+}−PA system established in ref6. at an inert salt level of

[NaCl] = 0.1 M. Although the scattering of the data points, which cover only a narrow regime of [PA], is considerable, we can state that the trend for the Cu^{2+}-system is compatible with a straight line pointing to the origin and hence with a distinct stoichiometic ratio of COO^- residues per Cu^{2+} ions. The slope of 0.29 ± 0.06 results in a ratio of 3 ± 1 COO^- per Cu^{2+}. Disregarding the large uncertainty for a moment, this value suggests that the chains may not exclusively be neutralized with Cu^{2+} cations as they precipitate. More important, the resulting trend is well below the corresponding phase boundary observed with the Ca^{2+}−PA system under identical conditions. With the Ca^{2+}−PA system, a clear extension of the one-phase state (dilute solution) is observed if the level of NaCl is increased.[6] This extension was interpreted due to an increasing excess of Na^+ ions causing a gradual exchange of the stronger bound Ca^{2+} . Apparently the binding of Cu^{2+} ions is much stronger than the Ca^{2+} ions and even a level of NaCl of 0.1 M does not succeed to significantly replace bound Cu^{2+} ions. Several values of the slopes were established for the phase boundary of the Ca^{2+}−PA system at [NaCl] = 0.1M, which indicate a stoichiometry close to 3:1.

Although, the present results do not totally exclude a Cu^{2+}/COO^- ratio of 1:2 for the precipitate postulated in the literature,[21,22] the precipitation threshold may already occur at a lower value for this ratio. As already outlined, shrinking may stop at a ratio of 1:4 corresponding to the kink of two trends in Figure 2, and, due to a much stronger interaction between Cu^{2+} and COO^- than between Ca^{2+} ions and COO^-, precipitation interferes with shrinking more readily in the former case. Thus, Cu^{2+}−PA may include more Na^+ ions as counterions in its precipitate than Ca^{2+}−PA does. The propensity of bound Ca^{2+} to be exchanged by an excess of Na^+ ions is considerably larger than of bound Cu^{2+} ions. This diminishes the stable one-phase regime of dilute solution of Cu^{2+}−PA. On a molecular level a larger extent of shrinking could be achieved in the case of Ca^{2+} than observed in the present work with Cu^{2+} by the time M^{2+}−PA is precipitating. The following paragraphs will address the question whether this causes differences in the mode of aggregation once the phase boundary is crossed.

The Onset of Aggregation. Crossing a phase boundary like the one indicated in Figure 5 for the systems under present investigation (i.e., Cu^{2+}−PA in 0.1 M NaCl) by increasing the Cu^{2+} content leads to macroscopically visible precipitates.[9−11] If the polyelectrolyte concentration is dilute enough, precipitation is preceded by a considerable coil shrinking, which may achieve a complete coil collapse in the case of Ca^{2+}−PA.[4,6] With these facts in mind, the interesting question arises whether an investigation of individually growing species with colloidal dimensions becomes possible in such cases? If it is possible to trace such a growth process of colloidal M^{2+}−PA aggregates, what can we learn about the morphology of these colloids and are there mechanistic differences between growing Cu^{2+}−PA aggregates and Ca^{2+}−PA aggregates?

TR-SLS is the method of choice to tackle these questions. To this end, dilute solutions of NaPA in the presence of appropriate amounts of $M^{2+} = Cu^{2+}$ or $M^{2+} = Ca^{2+}$ were prepared in 0.1 M NaCl. First, in solutions close enough to the phase boundary the ratio $[M^{2+}]/[PA]$ was increased in steps by adding small portions of concentrated M^{2+} solutions. Each stage was analyzed by TR-SLS. If the solution was stable for minutes the next portion of M^{2+} was added, respectively. At a certain M^{2+} content, the solution turned instable and exhibited a gradual increase in particle size and mass.

Figure 6 illustrates this procedure at a NaPA concentration of 0.21 mmol/L with Cu^{2+} the specifically interacting cation to be added. Addition of the initial amount of Cu^{2+} led to an instantaneous decrease of R_g and did hardly affect the apparent mass data M_w. Further details can be taken from Table 1 where this experimental series is denoted as Cu01. Addition of a second portion of Cu^{2+} slightly increased the particle dimensions and enlarged the particle mass by a factor of 2−3. Although this may already indicate formation of some small oligomers, the sample is still stable for more than 10 min. We also have to keep in mind that part of the increase in the mass may stem from the adsorption of Cu^{2+} ions, which does not only increase the mass but may also modify the scattering contrast of the objects. Only after addition of the third increment of Cu^{2+}, did an aggregation set in. The growth process under these conditions could be followed by TR-SLS for more than 10 min with a particle size of some 200 nm at the end of the experiment. The sample was not stable and eventually became turbid. The pathway of crossing the precipitation threshold also denoted as phase boundary is indicated in the inlet of Figure 6.

In order to further illuminate this growth process, the square root of the *z*-averaged mean square radius of gyration R_g of the growing particles was correlated with the corresponding weight-averaged particle mass indicated as M_w. At this point, we have to emphasize that particle mass values are only apparent values as the index of refraction of this Cu^{2+}−PA species is not known exactly and the value of NaPA in 0.1 M NaCl has been used instead. Such a correlation may lead to a power law according to eq9

$$R_g \propto M_w^a \tag{9}$$

Self-similar structures with a mass distribution independent of M_w exhibit an exponent a which is a characteristic value for the respective topology of the particles. For densely packed spheres or cubes the exponent has a value of $a = {}^1/_3$ and for ideal polymer coils or rods this value is ${}^1/_2$ or 1, respectively. If the resulting correlation is based on data recorded by static light scattering, R_g and M_w are averaged values, which include all species. In the case of a monomer addition mechanism, where monomers add to aggregates, monomers and aggregates are the only existing species. The "monomers" here correspond to single M^{2+}−Pa chains and the growing particles are aggregates thereof. Under such circumstances the monomer addition mechanism leads to exponents which are only half of the topological values, i. e. ${}^1/_2$ for rods, ${}^1/_4$ for ideal polymer coils, and ${}^1/_6$ for homogeneous spheres.[26] Topological exponents like ${}^1/_3$ for spheres may also be recovered from light scattering data if, in a coagulation process, any sphere-like aggregate particle can attach to any other particle independent from the degree of aggregation.[26]

The correlation, resulting from the experiments outlined in Figure 6 is represented in Figure 7. In fact, a power law with an exponent of 0.4 can clearly be discerned from the experimental data recorded after crossing the phase boundary. This trend could be fully reproduced with a second time-resolved experiment leading to an exponent of 0.42. Data of this second run denoted as Cu02 are shown in the Supporting Information. Exponents between 0.4 and 0.5 definitely exclude the formation of compact spherical particles even if aggregation would not follow a monomer addition mechanism but rather would take place as coagulation to ever larger spherical particles.[26] A value close to 0.4 also excludes aggregation following a monomer addition mechanism for a coil-like morphology as the latter mechanism would inevitably

result in an exponent equal to or smaller than 0.33. The fact that the value of the exponent is only slightly smaller than the one expected for particles with fractal dimensions of flexible polymer coils, leaves us with a coagulation process of coiled aggregates. This is also the more likely process to occur as an entangled dimer may just as well add to another dimer as it does to a monomer. A monomer addition mechanism toward rod-like aggregates is also compatible with an exponent close to 0.5 but appears to be extremely unlikely in the light of the coil-like structure of the constituent units.

A closer look onto the particle form factors of intermediate aggregates represented in Figure 8 nicely supports the scheme of coil-like structures. Such coil-like structures can be described by the Debye formula,[31] which in fact fits perfectly well to the experimental data once a polydispersity index of PDI = 2 is assumed. Polydispersity was taken into account by a Schulz−Zimm distribution[23,32] of the particle mass with a polydispersity parameter $z = 1$. This parameter is related to the polydispersity index PDI according to

$$z = 1/(\mathrm{PDI}-1) = M_n/(M_w - M_n) \qquad (10)$$

with $\mathrm{PDI} = M_w/M_n$ the ratio of the weight-averaged particle mass to the number-averaged particle mass. A Kratky plot of the respective form factors exhibit the beginning of a plateau value which is characteristic for coils.[27] Figure 8 also excludes the possibility of a monodisperse coil.

The aggregation behavior of Cu^{2+}−PA shall now be compared with the corresponding behavior of Ca^{2+}−PA. To this end, one series of experiments denoted as Ca03 has been performed in 0.1 M NaCl with a similar concentration of NaPA as used for the two experiments with Cu^{2+}−PA. Results from the Ca03 series are shown in Figure 9. In the first place, a much higher concentration is required for Ca^{2+} to cross the phase boundary than for Cu^{2+}. Two additional features are striking: (i) Particle mass values are larger by an order of magnitude if compared to those achieved in the corresponding experiments with Cu^{2+}. (ii) The exponent observed for the experiment Ca03-b is close to $^1/_3$ (Figure 7). If the same line of argumentation is followed as presented for the Cu^{2+} system, a coagulation mechanism is the more likely one to occur and hence an exponent close to $^1/_3$ indicates the formation of compact, spherically shaped aggregates. Figure 9 compares the growth curve of the Ca^{2+}−PA aggregates recorded at the low NaPA concentration close to 0.2 mM (Ca03) with another one, recorded at a NaPA concentration close to 1 mM (Ca04). As is shown in Figure 7, both sets of R_g versus M_w data are close to each other and reveal the same exponent.

The structural difference of Ca^{2+}-aggregates from Cu^{2+}-aggregates could be supported by an inspection of the particle form factors and of the structure-sensitive ratio of the radius of gyration and the hydrodynamically effective radius. The Kratky plot of the formfactors exhibits a clear maximum characteristic for regularely branched polymers or even spherical particles. This is a striking difference to the feature of the aggregates formed from Cu^{2+}−PA. As is demonstrated in Figure 10, the experimental curves of Ca^{2+}−PA aggregates from the experiment Ca03-b which are large enough to become shape sensitive can be overlaid and resemble the theoretical formfactor of a polydisperse sphere over a wide range of the normalized momentum transfer qR_g irrespective of the time-resolved experiment from which the curve was selected. The polydisperse formfactor was calculated with the formula derived by Rayleigh for monodisperse spheres[33] subdued to a Schulz−Zimm distribution[23] of the sphere volume with PDI = 2 according to eq10.

In experiment Ca04-b performed at 0.953 mM of NaPA, we succeeded to achieve a comparatively low growth rate. This enabled us to interrupt the TR-SLS experiment for about 14 min and perform a combined SLS and DLS analysis of the solution in the very cell. Comparison of the resulting hydrodynamically effective radius R_h from DLS with the radius of gyration yield $\rho = R_g/R_h = 0.77$, which is in line with expectations for a compact particle like a sphere.

As a consequence, Cu^{2+}−PA coils with a comparatively low final degree of shrinking (i.e., a comparatively large final value of $\alpha_g \sim 0.5$) form loose coil-like aggregates. The aggregates from Ca^{2+}−PA coils, on the other hand, form sphere-like aggregates, which are much more compact than the corresponding Cu^{2+}−PA aggregates. This could have been expected already from the shrunken Ca^{2+}−PA coils, which in their final conformation, are much more compact than the shrunken Cu^{2+}−PA coils.

An explanation of this behavior has to be related to the nature of the complex bond formation between the bivalent metal cations M^{2+} and the COO^- residues. A suitable characterization of such a complex bonding has been carried out by Miyajima et al.,[34] who considered polyelectrolyte solutions as domains, occupied by polyelectrolyte coils, which are separated by a polymer free solution phase. Miyajima et al.[34] applied the Donnan model to the domains of the anionic PA coils and an intrinsic complex formation constant was introduced by their eq9 of ref 34, for the complexation of Ca^{2+} and Cu^{2+} to COO^- residues within these coil domains. Following this concept, Miyajima et al.[34] could demonstrate, that at complete hydrolysis of the NaPA chains this intrinsic complex formation constant is larger for Cu^{2+} by more than 2 orders of magnitude than the respective formation constant for Ca^{2+}. Unlike Ca^{2+}, Cu^{2+} exhibits an increasing extent of coordination with two COO^- residues once the degree of hydrolysis exceeds 20%. This can be related to the occurrence of a binucleate Cu^{2+} complex established by Konrad and Rühe[16] in addition to a less stable mononucleate complex. The binucleate complex requires more than one COO^- ligand and complexes with more than one COO^- ligand per Cu^{2+} enable formation of intramolecular bridges between remote segments. The driving force of the less stable Ca^{2+} binding to COO^- residues could unambiguously be attributed to the liberation of H_2O molecules from solvation shells of the ions.[35] This entropic nature of Ca^{2+} binding was unraveled by means of calorimetric titration[35] and could later be confirmed by a molecular dynamics study.[36] These molecular dynamics simulation also revealed a frequent bonding of one Ca^{2+} by two neighboring COO^- residues. Such bonding stiffens the chain on a local length scale only and leads to a considerable electrical discharge of the chain backbone.[36] While putting these pieces of information together, we may extract the following reaction pattern. Cu^{2+} ions form coordination bonds to COO^- residues more vigorously and with a higher stability and with a higher propensity to bridging than Ca^{2+} ions do. This bridging generates intramolecular and intermolecular cross-links. The Cu^{2+}-induced cross-links occur long before the chains are fully neutralized and thus long before they are transformed into a hydrophobic, insoluble state. Hence, these cross-links kinetically arrest conformations in loosely shrunken and loosely aggregated states. In the presence of Ca^{2+}, the anionic PA chains will be decorated with M^{2+} more gradually and, as a result, to a much larger extent than in the case of Cu^{2+}. The resulting morphological changes do not get trapped in conformational states with low segment

density as easily as if arrested by stable coordinative cross-links with Cu^{2+}. Therefore, shrinking and aggregation induced by Ca^{2+} resembles the shrinking process observed with neutral polymer chains after crossing the Θ-state[37−39] and the respective processes induced by Cu^{2+} are comparable to an intermolecular and intramolecular cross-linking.

The present findings may be related to time-resolved DLS experiments on the aggregation of partially hydrolyzed polyacrylamide chains[40] induced by Ca^{2+} ions in salt free water. These experiments led to exponents close to $a = 0.48$ for eq9 which indicate a fractal dimension close to the one expected for polymer coils and are much closer to the size versus mass correlation found for the Cu^{2+} cations than for Ca^{2+}−NaPA in 0.1 M NaCl. Peng and Wu[40] used a degree of hydrolyzation of the polyacrylamide chains, which is fairly low. Only 20% of the residues were carboxylate functions at the most and thus ready to form complex bonds to Ca^{2+} ions and the remaining amide residues were less polar than the COO^- groups of the fully hydrolyzed NaPA chains. Apparently, these features led to a similar pattern of interchain cross-linking as induced by the Cu^{2+} ions with the fully hydrolyzed NaPA in 0.1 M NaCl.

Summary

Addition of Cu^{2+} ions to dilute solutions of high molecular weight NaPA chains induces a drastic shrinking of the NaPA chains. Unlike the corresponding effects observed with Ca^{2+} ions, the location of this shrinking in a phase diagram is hardly influenced by the presence of 0.1 M NaCl. NaCl considerably shifts the phase boundary of Ca^{2+}−PA solutions.[6] Hence the Cu^{2+}−PA complexes respond less sensitive to the pressure of ion exchange than the Ca^{2+}−PA complexes do. An additional difference between the impact of Cu^{2+} and Ca^{2+} cations observed with increasing the respective cation content is that the maximum extent of shrinking for the Cu^{2+}−PA coils is smaller than the one reached for the Ca^{2+}−PA coils by a factor of 2. Apparently, the Cu^{2+}−PA coils aggregate long before the limiting shape of a compact sphere is achieved and the shrinking induced with Ca^{2+} led to compact Ca^{2+}−PA spheres prior to crossing the phase boundary. This behavior influences the morphology of the resulting aggregates after crossing the phase boundary.

We unambiguously demonstrate by means of time-resolved static light scattering, that Cu^{2+}−PA aggregates grow as loose coil-like aggregates and Ca^{2+}−PA aggregates are much more compact objects similar to sphere-like shapes if aggregate formation is performed under identical conditions. As a consequence, the present findings suggest the application of specifically interacting cations as a new tool to control formation and morphology of polyacrylate aggregates.

Acknowledgment. The authors are indebted to M. Maxisch and S. Töws for their assistance in performing the shrinking experiments. Financial support of the Deutsche Forschungsgemeinschaft (grant HU807/7) is gratefully acknowledged.

Supporting Information Available: Figures showing the regime of validity of Zimm and Guinier analysis to model scattering curves and proof of reproducibility of the aggregation experiments with Cu^{2+}−PA and with Ca^{2+}−PA in aqueous 0.1 M NaCl solutions. This material is available free of charge via the Internet at http://pubs.acs.org.

References and Notes

(1) Takahashi, A.; Nagasawa, M. *J. Am. Chem. Soc.* **1964**, *86*, 543–548.
(2) Wang, L.; Yu, H. *Macromolecules* **1988**, *21*, 3498–3501.
(3) Schweins, R.; Hollmann, J.; Huber, K. *Polymer* **2003**, *44*, 7131–7141.
(4) Huber, K. *J. Phys. Chem.* **1993**, *97*, 9825–9830.
(5) Francois, J.; Truong, N. D.; Mehjadhi, G.; Mestdagh, M. M. *Polymer* **1997**, *38*, 6115–6127.
(6) Schweins, R.; Huber, K. *Eur. Phys. J E* **2001**, *5*, 117–126.
(7) Schweins, R.; Lindner, P.; Huber, K. *Macromolecules* **2003**, *36*, 9564–9573.
(8) Schweins, R.; Goerigk, G.; Huber, K. *Eur. Phys. J. E* **2006**, *21*, 99–110.
(9) Michaeli, I. *J. Polym. Sci.* **1960**, *48*, 291–299.
(10) Ikegami, A.; Imai, N. *J. Polym. Sci.* **1962**, *56*, 133–152.
(11) Narh, K. A.; Keller, A. *J. Polym. Sci.* **1993**, *31*, 231–234.
(12) Axelos, M. A. V.; Mestdagh, M. M.; Francois, J. *Macromolecules* **1994**, *27*, 6594–6602.
(13) Huber, K.; Witte, T.; Hollmann, J.; Keuker-Baumann, S. *J. Am. Chem. Soc.* **2007**, *129*, 1089–1094.
(14) Flory, P. J.; Osterheld, J. E. *J. Phys. Chem.* **1954**, *58*, 653–661.
(15) Heitz, C.; Francois, J. *Polymer* **1999**, *40*, 3331–3344.
(16) Konradi, R.; Rühe, R. *Macromolecules* **2005**, *38*, 4345–4354.
(17) Yokoi, H.; Kawata, S.; Iwaizumi, M. *J. Am. Chem. Soc.* **1986**, *108*, 3361–3365.
(18) Francois, J.; Heitz, C.; Mestdagh, M. M. *Polymer* **1997**, *38*, 5321–5331.
(19) Konradi, R.; Rühe, R. *Macromolecules* **2004**, *37*, 6954–6961.
(20) Iatridi, Z.; Bokias, G.; Kallitsis, J. K. *J. Appl. Polym. Sci.* **2008**, *108*, 769–776.
(21) Ikeda, Y.; Beer, M.; Schmidt, M.; Huber, K. *Macromolecules* **1998**, *31*, 728–733.
(22) Koppel, D. E. *J. Chem. Phys.* **1972**, *57*, 4814–4820.
(23) Zimm, B. *J. Chem. Phys.* **1948**, *16*, 1093−1099. Zimm, B. *J. Chem. Phys.* **1948**, *16*, 1099−1116.
(24) Becker, A.; Schmidt, M. *Macromol. Chem. Macromol. Symp.* **1991**, *50*, 249.
(25) Guinier, A. ; Fournet, G. *Small-Angle Scattering of X-Rays*; Wiley: New York, 1955; Chapter 4.1.1.
(26) Liu, J.; Rieger, J.; Huber, K. *Langmuir* **2008**, *24*, 8262–8271.
(27) Burchard, W. *Adv. Polym. Sci.* **1983**, *48*, 1−124 (see Chapter D therein).
(28) Schmidt, M.; Burchard, W. *Macromolecules* **1981**, *14*, 210–211.
(29) Dobrynin, A. V.; Rubinstein, M.; Obukhov, S. P. *Macromolecules* **1996**, *29*, 2974–2979.
(30) Wu, C.; Zhou, S. *Macromolecules* **1995**, *28*, 5388. Wu, C.; Zhou, S. *Macromolecules* **1995**, *28*, 8281.
(31) Debye, P. *J. Colloid Chem.* **1947**, *51*, 18–32.
(32) Greschner, G. S. *Makromol. Chem.* **1973**, *170*, 203–229.
(33) Rayleigh, L. *Proc. R. Soc. London* **1914**, *A90*, 219–225.
(34) Miyajima, T.; Mori, M.; Ishiguo, S.-I. *J. Colloid Interface Sci.* **1990**, *187*, 259–266.
(35) Sinn, C. G.; Dimora, R.; Antonietti, M. *Macromolecules* **2004**, *37*, 3444–3450.
(36) Bulo, R. E.; Donadio, D.; Laio, A.; Molnar, F.; Rieger, J.; Parrinello, M. *Macromolecules* **2007**, *40*, 3437–3442.
(37) Sun, S.-T.; Nishio, I.; Swislow, G.; Tanaka, T. *J. Phys. Chem.* **1980**, *73*, 5971–5975.
(38) Chu, B.; Ying, Q.; Grosberg *Macromolecules* **1995**, *28*, 180–189.
(39) Kuznetsov, Y. A.; Timoshenko, E. G.; Dawson, K. A. *J. Chem. Phys.* **1995**, *103*, 4807–4818.
(40) Peng, S.; Wu, C. *Macromolecules* **1999**, *32*, 585–589.